EPJ Web of Conferences **312**, 05003 (2024) https://doi.org/10.1051/epjconf/202431205003
FPCP 2024

Asymmetric Self-interacting Dark Matter and Neutrino Mass via Dirac Leptogenesis

Manoranjan Dutta[1,*] and *Nimmala* Narendra[2,**]

[1]Department of Physics, North Lakhimpur University, Khelmati, North Lakhimpur, Lakhimpur, Assam 787031, India
[2]Indian Association for the Cultivation of Science (IACS), Kolkata, Jadavpur, 700032, West Bengal, India

Abstract. We propose a framework to address the observed baryon asymmetry considering neutrinos as Dirac particles and dark matter to be self-interacting. The Standard Model is extended by $U(1)_{B-L} \times U(1)_D$ symmetry. In addition to the three right-handed neutrinos, the Standard Model particle content is extended by two more fermion fields; one of them is a $SU(2)$ singlet and the other one is $SU(2)$ doublet, both charged under the extended symmetry. A Z_2 symmetry is imposed under which the doublet is positive while the singlet is negative. The singlet, being the lightest dark sector particle, acts as the dark matter. The $U(1)_D$ symmetry of the dark sector is spontaneously broken and the corresponding gauge boson Z' not only mediates the self-interaction among dark matter particles, but also facilitates the annihilation of the symmetric component of dark matter. CP-violating out of equilibrium decay of another heavy Z_2 odd $SU(2)$ scalar doublet N into leptonic and dark sectors produce the observed baryon asymmetry and dark matter density. Moreover, Z' also mixes with the standard model Z-boson opening up a portal for the direct detection of dark matter.

1 Introduction

The standard model (SM) of particle physics fails to explain several issues like neutrino mass, dark matter (DM) and the observed baryon asymmetry. Within the SM, neutrinos are massless due to absence of right handed neutrino field. However, neutrino flavour oscillation demonstrated by the oscillation experiments [1–10] hints towards a tiny neutrino mass of sub-eV scale. Moreover, whether neutrino is a Dirac or Majorana fermion is still unsettled. The lepton number violating interactions ($\Delta L = 2$) indicative of Majorana nature of neutrinos is being probed at ongoing neutrinoless double beta decay experiments [11]. However there is no confirmatory results yet. Therefore, the possibility of neutrinos being a Dirac fermion is still alive. The galaxy rotation curves, gravitational lensing, anisotropies in the Cosmic Microwave Background (CMB) *etc.* hint towards the existence of dark matter (DM), an electromagnetically inert form of matter. Data from satellite borne experiments, such as WMAP [12] and PLANCK [13] suggests that the DM is about five times more abundant than

*e-mail: dutta.manoranjan@nlc.ac.in
**e-mail: nimmalanarendra@gmail.com

© The Authors, published by EDP Sciences. This is an open access article distributed under the terms of the Creative Commons Attribution License 4.0 (https://creativecommons.org/licenses/by/4.0/).

the baryons, *i.e.,* $\Omega_{\rm DM} \approx 5\Omega_{\rm B}$. Moreover, the present universe is highly baryon asymmetric, leading to yet another puzzle known as the baryon asymmetry of universe (BAU). The observed BAU is quantitatively expressed by the ratio of baryon density over anti-baryons density to photon density as [13], $\eta_B = \frac{n_B - n_{\overline{B}}}{n_\gamma} \simeq 6.2 \times 10^{-10}$.

From the cosmological perspective, the ΛCDM model has been enormously successful in explaining the large-scale structures of the universe. This model incorporates DM too and assumes it to be a cold and collisionless fluid. However, at smaller scales, quite a few discrepancies of ΛCDM predictions have emerged *e.g.* the core-cusp problem, the missing satellite problem and the too-big-to-fail problem *etc* [14, 15]. These discrepancies are more prominent at the scale of dwarf galaxies and decreases gradually towards the cluster scale matching with ΛCDM predictions at large scale. To alleviate these anomalies, self-interacting dark matter (SIDM)[16–18] was proposed as an alternative to conventional cold dark matter. It has been shown that a velocity-dependent DM self-interaction with a cross-section of the order of $\sigma/m \sim 1\ \text{cm}^2/\text{g} \approx 2 \times 10^{-24}\ \text{cm}^2/\text{GeV}$ can alleviate these anomalies[19–29]. DM models with a light mediator is well suited to realise such velocity dependent cross-section [30–35].

In this paper we make an attempt to explain the observed BAU assuming neutrinos to be Dirac fermions and DM to be self-interacting. Considering neutrinos to be Dirac particles implies $B-L$ is an exact symmetry of the universe. Then the observed BAU can be explained by the frameworks of Dirac leptogenesis [36–40]. The basic mechanism of Dirac Leptogenesis is that the equilibration time between left-handed neutrinos (ν_L) and right-handed neutrinos (ν_R) mediated by SM Higgs via Yukkawa interaction of the form $Y\overline{L}H\nu_R$, where $L = (\nu_l, l)^T$ represents SM lepton doublet, is much less than the $(B + L)$ violating sphaleron transitions above electroweak phase transition. Therefore, demanding $B-L = B-(L_{\rm SM}+L_{\nu_R}) = 0$[37], a net $B-L_{\rm SM}$ can be cooked in terms of L_{ν_R}. As ν_R is $SU(2)_L$ singlet, L_{ν_R} remains unaffected by electroweak sphalerons. The non-zero $B - L_{\rm SM}$ is, however, converted to a net B asymmetry via $B + L$ violating sphaleron transitions.

The paper is organized as follows. In sec. 2, we discuss the proposed model, while in sec. 3, we explain the Dirac masses of light neutrinos. Section 4 is devoted to explain baryogenesis via leptogenesis from the decay of heavy particles N, while section 5 describes the origin of observed DM abundance. Other phenomenologies related to DM *e.g.* self-interaction, direct detection *etc.* are discussed in section 6. We finally summarise and conclude in sec. 7.

2 The Model

We extend the SM with two vector-like leptons, one of them is a $SU(2)_L$ singlet χ and the other one is a $SU(2)_L$ doublet ψ. The dark sector is gauged under a softly broken $U(1)_D$ symmetry, with the gauge boson Z' having a MeV scale mass. The singlet fermion, χ being the lightest particle in the dark sector, acts as the DM candidate. A heavy scalar doublet N and three right handed neutrinos ν_{R_α}, $\alpha = 1, 2, 3$ are also introduced. A discrete symmetry Z_2 is also imposed under which N, ν_R and χ are odd, while ψ and all other SM particles are even. ψ and χ also carry non-trivial quantum numbers under $U(1)_D$ symmetry. As a consequence, the trilinear couplings $\bar{\psi}N\nu_R$ and $\bar{L}N\chi$ are forbidden. The overall $B - L$ global symmetry remains intact as the neutrinos are assumed to be Dirac particles. The BSM particle content and their charge assignments are shown in Table 2.

The CP-violating out-of-equilibrium decay of heavy scalar N creates asymmetries simultaneously in both lepton and dark matter sectors [41]. In the visible sector, the decay of N to ℓ and ν_R, creates an equal and opposite lepton asymmetry in both left and right-handed sectors. The lepton asymmetry in the left-handed sector gets converted to a net baryon asymmetry

Parameter	$U(1)_{B-L}$	$U(1)_D$	Z_2
$N = (N^+, N^0)^T$	0	0	-
ν_R	-1	0	-
$\psi = (\psi^0, \psi^-)^T$	-1	1	+
χ	-1	1	-

Table 1. New particles and their charges under the extended symmetry.

through $B+L$ violating sphaleron transitions, while the asymmetry in the right-handed sector remains unaffected until the temperature falls much below the electroweak phase transition. Note that the coupling $\bar{L}H\nu_R$ and $\bar{\psi}H\chi$ are forbidden due to Z_2 symmetry.

The doublet ψ remains in thermal equilibrium in the early universe. The DM candidate χ, although a $SU(2)_L$ singlet, attains thermal equilibrium via the process $\psi\psi \to \chi\chi$, mediated by the light mediator Z'. However, the thermal relic of χ is negligible as it annihilates efficiently via t-channel into pairs of Z'. Hence, there is negligible symmetric relic and the observed DM relic density is produced by the CP-violating out-of-equilibrium decay of heavy scalar N. Z' also facilitates the self scattering among the DM. The kinetic mixing between $U(1)_Y$ and $U(1)_D$ enables the direct detection of DM in terrestrial laboratories. Fig. 1 depicts the Feynman graphs for annihilion channel, self-interaction and direct search of DM.

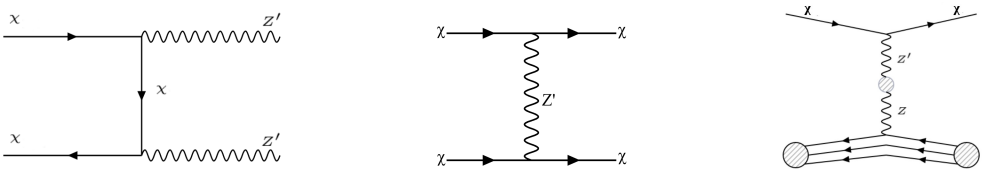

Figure 1. Feynman graphs depicting dominant annihilation channel, self-interaction and direct detection channel.

The relevant Lagrangian for the model can be written as:

$$\begin{aligned}\mathcal{L} \supset\ & \bar{\psi} i\gamma^\mu D_\mu \psi + \bar{\chi} i\gamma^\mu D'_\mu \chi + M_\psi \bar{\psi}\psi + M_\chi \bar{\chi}\chi - \mu^2 H^\dagger N + \text{h.c.} \\ & + \left[\lambda_l \bar{L}\tilde{N}\nu_R + \lambda_d \bar{\psi}\tilde{N}\chi + \text{h.c.}\right] - V(H, X)\,. \end{aligned} \tag{1}$$

where

$$\begin{aligned} D_\mu &= \partial_\mu - i\frac{g}{2}\tau^i W^i_\mu - i\frac{g'}{2} Y B_\mu - i g_D Z'_\mu \\ D'_\mu &= \partial_\mu - i g_D Z'_\mu \end{aligned} \tag{2}$$

and the scalar potential is given by,

$$\begin{aligned} V(H, N) = & -M_H^2 H^\dagger H + M_N^2 N^\dagger N + \lambda_H (H^\dagger H)^2 \\ & + \lambda_N (N^\dagger N)^2 + \lambda_{HN} (H^\dagger H)(N^\dagger N) \end{aligned} \tag{3}$$

3 Dirac mass of neutrinos

The imposed Z_2 symmetry is softly broken [44, 45] by the term:

$$\mathcal{L}_{soft} = -\mu^2 H^\dagger N + \text{h.c.} \tag{4}$$

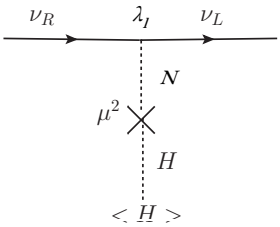

Figure 2. Dirac mass of neutrinos generated via soft Z_2 breaking.

Consequently, the Dirac mass of the neutrinos can be generated as shown in the Fig. 2. After integrating out the heavy scalar field N we get the Dirac neutrino mass:

$$M_\nu = \frac{\lambda_l \langle H \rangle \mu^2}{M_N^2}\,, \tag{5}$$

where $\langle H \rangle = 174$ GeV, is the vacuum expectation value (VEV) of the SM Higgs. From Eq. 5, to generate Dirac neutrino mass of order 0.1 eV, we need $\frac{\mu}{M_N} \approx 10^{-4}$ assuming that $\lambda_l \sim 10^{-4}$. The smallness of μ in comparison to the mass scale of heavy scalar doublet N justifies the soft breaking of Z_2 symmetry.

4 Baryogenesis via Dirac Leptogenesis

At temperature above its mass scale, the heavy scalar N is in thermal equilibrium, thanks to its gauge and Yukawa interactions. As temperature falls due to Hubble expansion, N goes out-of-thermal equilibrium below its mass scale, and decays into both visible ($l\nu_R$) and dark sectors ($\psi\chi$). The decay rate of N-particle is given by:

$$\Gamma_N \simeq \frac{1}{8\pi}(\lambda_l^2 + \lambda_d^2) M_N\,, \tag{6}$$

where λ_l and λ_d are Yukawa couplings of N to leptons and dark sectors respectively. Demanding that $\Gamma_N \lesssim H$ at $T = M_N$, where $H = 1.67 g_*^{1/2} T^2/M_{\rm Pl}$ is the Hubble expansion rate, we get $M_N \lesssim 10^{10}$ GeV for $\lambda_l \sim \lambda_d \lesssim 10^{-4}$. The CP-violating decay of N requires at least two copies of N. We assume a mass hierarchy between the two copies of N-particles so that the CP-violating decay of the lightest N to $\ell\nu_R$ and $\psi\chi$ generates asymmetries in both the sectors. The decay modes to visible sector are $N^0 \to \nu_L \nu_R$ and $N^- \to \ell^- \nu_R$, while the decay modes to dark sector are $N^0 \to \psi^0\chi$ and $N^- \to \psi^-\chi$. The two decay modes of N in each sector are equivalent and hence we will focus only one of the channels, say $N^- \to \ell^-\nu_R$ in the visible sector and $N^- \to \psi^-\chi$ in the dark sector.

In presence of pairs of doublet scalars N and their interactions, we get a mass matrix $M_\pm^2$, diagonalizing which, we get two mass eigenvalues M_{ξ_1} and M_{ξ_2} corresponding to two eigenstates $\xi_1^\pm$ and $\xi_2^\pm$ (See for more details [41, 46]). Their decays give rise to CP-asymmetry via the interference of tree level and one-loop self-energy correction diagrams shown in Fig. 3. The asymmetry generated in the visible sector can be quantified as,

$$\begin{aligned} \epsilon_L &= [B_L(\xi_1^- \to l^- \nu_R) - B_L(\xi_1^+ \to (l^-)^c \nu_R^c)] \\ &= -\frac{Im\left((\lambda_d)_1^* (\lambda_d)_2 \sum_{\alpha\beta} (\lambda_l)_{1\alpha\beta}^* (\lambda_l)_{2\alpha\beta}\right)}{8\pi^2 (M_2^2 - M_1^2)} \left[\frac{M_1^2 M_2}{\Gamma_1}\right], \end{aligned} \tag{7}$$

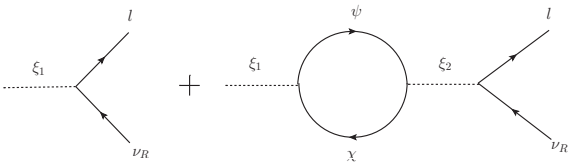

Figure 3. Tree level and self energy correction diagrams, whose interference give rise to a net CP violation.

where B_L is the branching ratio for $\xi_1^{\pm} \to l^{\pm}\nu_R$. Using the CP-asymmetry parameter ϵ_L, we can estimate the generated lepton asymmetry $Y_L \equiv \frac{n_L}{s}$, where $s = (2\pi^2/45)g_* T^3$ is the entropy density. The relevant Boltzmann equations governing the evolution of the number density of ξ_1 and the lepton asymmetry Y_L in terms of are given by:

$$\begin{aligned}\frac{dY_{\xi_1}}{dx} &= -\frac{x}{H(M_{\xi_1})} s < \sigma|v|_{(\xi_1\xi_1 \to All)} > \left[Y_{\xi_1}^2 - Y_{\xi_1}^{eq2}\right] \\ &\quad - \frac{x}{H(M_{\xi_1})}\Gamma_{(\xi_1 \to All)}\left[Y_{\xi_1} - Y_{\xi_1}^{eq}\right] \\ \frac{dY_L}{dx} &= \epsilon_L \frac{x}{H(M_{\xi_1})}\Gamma_{(\xi_1 \to All)} B_L \left[Y_{\xi_1} - Y_{\xi_1}^{eq}\right] \end{aligned} \tag{8}$$

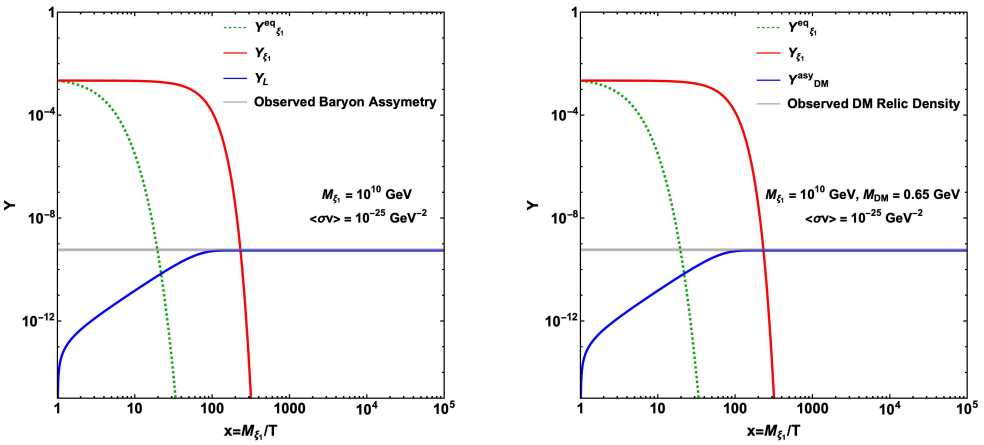

Figure 4. [Left]: The lepton asymmetry from the decay of ξ_1. The Green(dotted) line shows the abundance of lepton asymmetry for $\epsilon_L = 2 \times 10^{-7}$. The Blue(dashed) line shows the abundance of ξ_1 particles. The Black solid line shows the equilibrium number density of ξ_1. [Right]: Evolution of asymmetric DM relic density.

We have shown in the left panel of Fig. 4, the lepton asymmetry Y_L and the comoving number density of ξ_1, *i.e.* Y_{ξ_1}. The decay coupling constant λ_l is taken as 10^{-4} and the λ_d is taken as 10^{-7}. The typical value of the cross-section is taken as $\sigma|v|_{(\xi_1\xi_1 \to All)} = 10^{-25} GeV^{-2}$. The solid red line shows the evolution of the number density of ξ_1 particles and the solid blue line depicts the evolution of lepton asymmetries. From Fig. 4, we see that as the temperature falls below the mass of ξ_1 (*i.e.* $x > 1$), it decouples from the thermal bath. As ξ_1 starts decaying to $\ell^- \nu_R$, the lepton asymmetry starts developing proportional to B_L and ϵ_L, and settles to a constant value after the decay of ξ_1 is complete. In Fig. 4, we have taken the

branching ratio $B_L \sim O(1)$ and $M_{\xi_1} = 10^{10}$ GeV. The electroweak sphalerons which violate $B+L$ (but conserves $B-L$) transfer a portion of lepton asymmetry to a net baryon asymmetry $Y_B = -0.55 Y_L$. For $\epsilon_L = 5 \times 10^{-7}$ and the parameters as discussed above, we get the required baryon asymmetry.

5 Asymmetric Dark matter and Relic Abundance

Due to electroweak gauge interactions, the vector-like fermion doublet ψ remains in thermal equilibrium at a temperature above its mass scale in the early universe. The number density of the symmetric component of ψ gets diluted by three annihilation processes: $\overline{\psi}\psi \rightarrow SM\ SM, \overline{\psi}\psi \rightarrow \overline{\chi}\chi, \overline{\psi}\psi \rightarrow Z'Z'$. The symmetric component of DM candidate χ (which is also in the thermal equilibrium due to the the process $\psi\psi \rightarrow \chi\chi$ mediated by the light vector boson Z'), undergoes thermal freeze-out via $\chi\chi \rightarrow Z'Z'$. The thermally averaged cross-section for this annihilation process can be estimated as,

$$\langle \sigma v \rangle_{\overline{\chi}\chi \rightarrow Z'Z'} \approx \frac{\pi \alpha_D^2}{M_\chi^2} \left(1 - \frac{M_{Z'}^2}{M_\chi^2}\right)^2 \tag{9}$$

where $\alpha_D = g_D^2/4\pi$. For $g_D \sim 0.1$ and DM mass $M_{DM} \sim 1$ GeV, this leads to a cross-section that is at least two orders of magnitudes larger than the typical WIMP annihilation cross section that yields correct relic density. The relic density of the symmetric DM component is under-abundant up to a DM mass ~1 TeV.

The asymmetric number density of ψ gets converted to a net χ density through the decay process: $\psi \rightarrow \chi \bar{f} f$, induced via the soft Z_2 symmetry breaking term $\mu^2 H^\dagger N$. The CP-violating out of equilibrium decays $\xi_1^- \rightarrow \xi^- \chi, \zeta_1^+ \rightarrow (\psi^-)^c \chi^c$ give rise to the desired DM relic density. These decays produce an asymmetry between χ and $\bar{\chi}$, as well as between ψ and $\bar{\psi}$. The corresponding tree level and self energy correction diagrams are shown in Fig. 5.

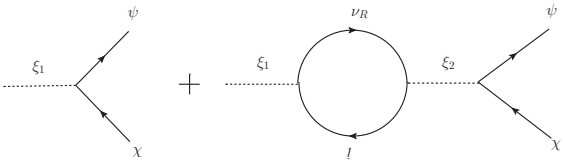

Figure 5. Tree level and self energy correction diagrams producing the dark matter asymmetry

The amount of CP-asymmetry can be quantified as,

$$\begin{aligned} \epsilon_\chi &= [Br(\xi_1^- \rightarrow \psi^- \chi) - Br(\xi_1^+ \rightarrow (\psi^-)^c \chi^c)] \\ &= \frac{Im\left((\lambda_d)_1^* (\lambda_d)_2 \sum_{\alpha,\beta} (\lambda_l)_{1\alpha\beta}^* (\lambda_l)_{2\alpha\beta}\right)}{8\pi^2 (M_2^2 - M_1^2)} \left[\frac{M_1^2 M_2}{\Gamma_1}\right] = -\epsilon_L. \end{aligned} \tag{10}$$

The abundance of asymmetric χ density from decay of ξ_1 and ξ_2 can be estimated from the Boltzmann equations:

$$\begin{aligned} \frac{dY_{\xi_1}}{dx} &= -\frac{x}{H(M_{\xi_1})} s < \sigma |v|_{(\xi_1 \xi_1 \rightarrow All)} > \left[Y_{\xi_1}^2 - Y_{\xi_1}^{eq2}\right] \\ &\quad - \frac{x}{H(M_{\xi_1})} \Gamma_{(\xi_1 \rightarrow All)} \left[Y_{\xi_1} - Y_{\xi_1}^{eq}\right], \\ \frac{dY_{\chi-\overline{\chi}}}{dx} &= \epsilon_\chi \frac{x}{H(M_{\xi_1})} \Gamma_{(\xi_1 \rightarrow All)} B_\chi \left[Y_{\xi_1} - Y_{\xi_1}^{eq}\right]. \end{aligned} \tag{11}$$

Here we use $|\epsilon_\chi| = |\epsilon_L| = 5 \times 10^{-7}$. Interestingly, for a DM of mass $m_\chi = 0.65$GeV, the required DM relic (Y_{DM}) matches exactly with the observed baryon asymmetry (Y_B). For better visualization, we show this case in the right panel of Fig. 4, where we use $\lambda_l = 10^{-4}, \lambda_d = 10^{-7}, \sigma|v|_{(\xi_1\xi_1 \to All)} = 10^{-25} GeV^{-2}$ (same values were used in Sec. 3 and Sec. 4). The solid red line shows the evolution of the number density of ξ_1 particles and the solid blue line depicts the evolution of $Y_{\chi-\bar{\chi}}$. Note that the decay $\xi_1 \to \psi\chi$ does not affect the observed baryon asymmetry. This is because, being vector-like fermions, ψ and χ are not disturbed by the sphalerons [41–43].

6 Dark Matter Self-interaction and Direct Search Constraints

The DM χ has elastic self-scattering, mediated by the MeV scale vector boson Z', thanks to the interaction term $g_D \bar{\chi}\chi Z'$ in the model Lagrangian given by Eq. 1. In the non-relativistic limit, this interaction is well-described by the attractive Yukawa potential,

$$V(r) = \pm \frac{g_D^2}{4\pi r} e^{-M_{Z'} r} \tag{12}$$

where, the + (-) sign denotes repulsive (attractive) potential. Here we will focus on the attractive potential. To capture the relevant physics of forward scattering divergence, we define the transfer cross-section σ_T as [14, 20, 29]

$$\sigma_T = \int d\Omega (1 - \cos\theta) \frac{d\sigma}{d\Omega} \tag{13}$$

Depending on the mass of DM (M_χ) and the mediator ($M_{Z'}$), as well as the relative velocity of the colliding particle (v) and the coupling (g_D^2), we can identify three distinct regimes. The Born regime ($g_D^2 M_\chi/(4\pi M_Z) \ll 1, M_\chi v/M_Z \geq 1$) is where the perturbative calculation holds good. Outside the Born regime, we have the classical regime ($g_D^2 M_\chi/(4\pi M_Z) \geq 1, M_\chi v/M_Z \geq 1$) and the resonant regime ($g_D^2 M_\chi/(4\pi M_Z) \geq 1, M_\chi v/M_Z \leq 1$) where non-perturbative and quantum-mechanical effects become important. The self-interaction cross-sections in these regimes are listed in Appendix A. In the left panel of Fig. 6, we show the self-interaction allowed parameter space in M_χ - M_Z plane obtained by constraining σ/M_χ in the correct ballpark from astrophysical data across different scales. We constrain σ/M_χ in the range $0.1 - 10$ cm^2/g for dwarf galaxies ($v \sim 10$ km/s) and galaxies ($v \sim 100$ km/s), and $0.1 - 1$ cm^2/g for clusters ($v \sim 1000$ km/s), considering $g_D = 0.1$. Three cases are depicted by shades of cyan, green and gray colours respectively as indicated in the figure inset. The top (bottom) corner corresponds to the Classical (Born) region, where the cross-section depends on velocity trivially. The sandwiched region between these two is the so-called resonant region, where quantum mechanical resonances and anti-resonances appear due to (quasi)bound state formation in the attractive potential. The self-scattering cross-section per unit DM mass as a function of average collision velocity obtained from the model fits to data from dwarfs (red), low surface brightness (LSB) galaxies (blue), and clusters (green) [26, 27] as shown in the right panel of Fig 6. The magenta coloured curve corresponds to the benchmark point of $M_\chi = 0.65$ GeV (depicted in the left panel of Fig. 4 with $M_Z = 0.006$GeV and $g_D = 0.1$. In comparison, the purple coloured curve corresponds to the benchmark point of $M_\chi = 5$ GeV with other parameters being same.

SIDM χ can be detected through its elastic scattering off the nucleons of the detector atoms via $Z - Z'$ kinetic mixing. The spin independent direct search cross section for a given nucleus N with proton number Z and mass number A is given by

$$\sigma_{\chi N}^{\rm SI} = \frac{g^2 g_D^2 \epsilon^2}{\pi} \frac{\mu_{\chi N}^2}{M_{Z'}^4} \frac{(Z f_p + (A - Z) f_n)^2}{A^2}. \tag{14}$$

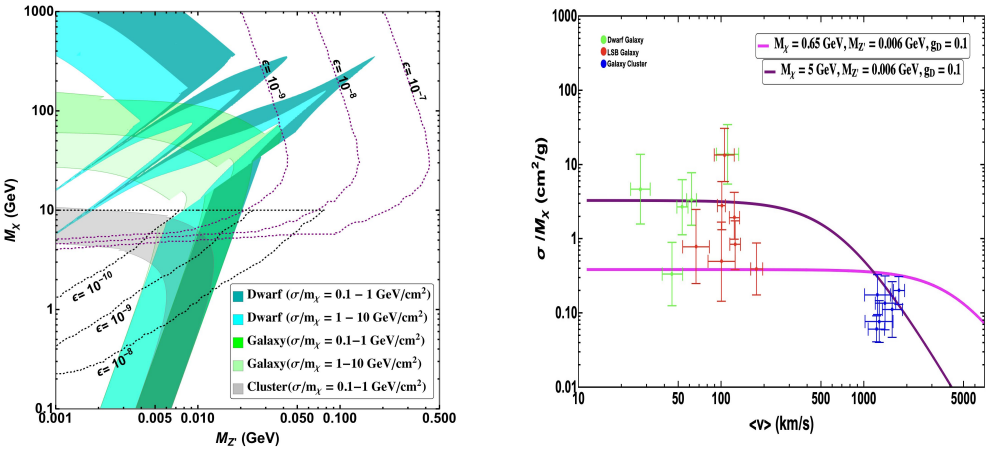

Figure 6. [Left]: Self-interaction cross-section allowed parameter space in the range $0.1 - 1$ cm^2/g for clusters ($v \sim 1000$ km/s), $0.1 - 10$ cm^2/g for galaxies and dwarf galaxies ($v \sim 10$ km/s). [Right]: The self-interaction cross-section per unit mass of DM as a function of average collision velocity.

where, $\mu_{\chi N} = \frac{m_\chi m_N}{(m_\chi + m_N)}$ is the reduced mass of the DM-nucleus system, ϵ is the $Z - Z'$ kinetic mixing, f_p and f_n are the interaction strengths for proton and neutron respectively. DM direct search experiments like CRESST-III [47] and XENON1T [48] constrains the model parameters. XENON1T (CRESST-III) provides the most stringent bound for DM of mass above (below) 10 GeV. The dotted black (purple) contours in the left panel of Fig. 6 shows the most stringent constraints from CRESST-III (XENON1T) experiments depicting the exclusion limits for the specific kinetic mixing parameter mentioned alongside each contour. The region towards the left of each contour is excluded by the current experimental data for that specific kinetic mixing parameter.

7 Conclusions

In this paper, exploiting the possibility of neutrinos being Dirac particles (*i.e.,* $B - L$ is an exact symmetry), we explain simultaneously neutrino mass, baryon asymmetry and the phenomenologies of SIDM. We extended the SM with a dark sector constituting vector-like fermion doublet ψ and singlet χ, where χ being odd under a discrete Z_2 symmetry, behaves as the DM candidate. The same Z_2 symmetry disallows Dirac neutrino mass by forbidding $\bar{\nu_R}\tilde{H}^\dagger L$ coupling, where ν_R is odd under the Z_2 symmetry. However, the discrete Z_2 symmetry was allowed to be broken softly without destabilizing the dark matter. Consequently, a Dirac mass of the active neutrinos could be generated. The out-of-equilibrium decay of a heavy scalar doublet N: $N \to \nu_R \ell$ and $N \to \chi\psi$ generated the observed baryon and dark matter asymmetry. The symmetric component of DM annihilates away into the $U(1)_D$ gauge boson Z', which also mediates self-interaction among DM particles that helps alleviate the small scale anomalies associated with ΛCDM model. The kinetic mixing between $U(1)_D$ and $U(1)_Y$ also opens a portal for the DM direct detection. We have found the relevant parameter space for self-interaction in terms of DM and mediator mass confronted with direct search constraints. The indirect signals of SIDM remains well below the current constraints by the experiments like Fermi-LAT, MAGIC, HESS, AMS-02 and INTEGRAL *etc.* [33]. We will study possible collider signatures of SIDM in a future work.

A DM Self-interaction Cross-sections at Low Energy

In the Born Limit ($g_D^2 M_\chi/(4\pi M_Z) << 1$),

$$\sigma_T^{Born} = \frac{g_D^4}{2\pi m_\chi^2 v^4}\left(ln(1+\frac{m_\chi^2 v^2}{m_\phi^2}) - \frac{m_\chi^2 v^2}{m_\phi^2 + m_\chi^2 v^2}\right) \tag{15}$$

Outside the Born regime ($g_D^2 M_\chi/(4\pi M_Z) \geq 1$), there are two distinct regions *viz*, the classical regime and the resonance regime. In the classical regime ($g_D^2 M_\chi/(4\pi M_Z \geq 1, M_\chi v/M_Z \geq 1$), the solutions for an attractive potential is given by[29, 49, 50]:

$$\sigma_T^{classical} = \begin{cases} \frac{4\pi}{m_\phi^2}\beta^2 ln(1+\beta^{-1}) & \beta \leqslant 10^{-1} \\ \frac{8\pi}{m_\phi^2}\beta^2/(1+1.5\beta^{1.65}) & 10^{-1} \leq \beta \leqslant 10^3 \\ \frac{\pi}{m_\phi^2}(ln\beta + 1 - \frac{1}{2}ln^{-1}\beta) & \beta \geq 10^3 \end{cases} \tag{16}$$

where $\beta = 2g_D^2 M_\chi/(4\pi M_Z)v^2$ In the resonant regime ($g_D^2 M_\chi/(4\pi M_Z) \geq 1, M_\chi v/M_Z \leq 1$), the quantum mechanical resonances and anti-resonance in σ_T appear due to (quasi-)bound states formation in the attractive potential. In the resonant regime, an analytical formula for σ_T is not available and one needs to solve the non-relativistic Schrodinger equation by partial wave analysis. Instead, here we use the non-perturbative results obtained by approximating the Yukawa potential to be a Hulthen potential $\left(V(r) = \pm\frac{g_D^2}{4\pi}\frac{\delta e^{-\delta r}}{1-e^{-\delta r}}\right)$, which is given by [29]:

$$\sigma_T^{Hulthen} = \frac{16\pi \sin^2\delta_0}{m_\chi^2 v^2} \tag{17}$$

where $l = 0$ phase shift δ_0 is given in terms of the Γ functions by :

$$\begin{aligned} \delta_0 &= arg\left(i\Gamma\left(\tfrac{iM_\chi v}{k\ M_Z}\right)\Big/\Gamma(\lambda_+)\Gamma(\lambda_-)\right) \\ \lambda_\pm &= 1 + \tfrac{iM_\chi v}{2\ k\ M_Z} \pm \sqrt{\tfrac{\alpha_D M_\chi}{kM_Z} - \tfrac{m_\chi^2 v^2}{4k^2 m_\phi^2}} \end{aligned} \tag{18}$$

and $k \approx 1.6$ is a dimensionless number.

References

[1] **T2K** Collaboration, K. Abe et al., Indication of Electron Neutrino Appearance from an Accelerator-produced Off-axis Muon Neutrino Beam, Phys. Rev. Lett. **107** 041801 (2011), https://doi.org/10.1103/PhysRevLett.107.041801

[2] **T2K** Collaboration, K. Abe et al., Observation of Electron Neutrino Appearance in a Muon Neutrino Beam. Phys. Rev. Lett. **112**, 061802 (2014). https://doi.org/10.1103/PhysRevLett.112.061802

[3] **Double Chooz** Collaboration, Y. Abe et al., Indication of Reactor $\bar{\nu}_e$ Disappearance in the Double Chooz Experiment. Phys. Rev. Lett. **108**, 131801 (2012). https://doi.org/10.1103/PhysRevLett.108.131801

[4] **Double Chooz** Collaboration, H. de Kerret et al., First Double Chooz θ_{13} Measurement via Total Neutron Capture Detection. Nature Phys. **16** (2020), no. 5 558–564. https://doi.org/10.1038/s41567-019-0720-1

[5] **Daya Bay** Collaboration, F. An et al., Observation of electron-antineutrino disappearance at Daya Bay. Phys. Rev. Lett. **108**, 171803 (2012). https://doi.org/10.1103/PhysRevLett.108.171803

[6] **Daya Bay** Collaboration, F. An et al., Evolution of the Reactor Antineutrino Flux and Spectrum at Daya Bay. Phys. Rev. Lett. **118** (2017), no. 25 251801. https://doi.org/10.1103/PhysRevLett.118.251801

[7] **Daya Bay** Collaboration, D. Adey et al., Measurement of the Electron Antineutrino Oscillation with 1958 Days of Operation at Daya Bay. Phys. Rev. Lett. **121** (2018), no. 24 241805. https://doi.org/10.1103/PhysRevLett.121.241805

[8] **RENO** Collaboration, J. Ahn et al., Observation of Reactor Electron Antineutrino Disappearance in the RENO Experiment. Phys. Rev. Lett. **108**, 191802 (2012). https://doi.org/10.1103/PhysRevLett.108.191802

[9] **MINOS** Collaboration, P. Adamson et al., Measurement of Neutrino and Antineutrino Oscillations Using Beam and Atmospheric Data in MINOS. Phys. Rev. Lett. **110** (2013), no. 25 251801. https://doi.org/10.1103/PhysRevLett.110.251801

[10] **MINOS** Collaboration, P. Adamson et al., Combined analysis of ν_μ disappearance and $\nu_\mu \to \nu_e$ appearance in MINOS using accelerator and atmospheric neutrinos. Phys. Rev. Lett. **112** (2014) 191801. https://doi.org/10.1103/PhysRevLett.112.191801

[11] O. Azzolini et al. (CUPID-0 collaboration), Measurement of the Electron Antineutrino Oscillation with 1958 Days of Operation at Daya Bay. Phys. Rev. Lett. **120**, 232502 (2018). https://doi.org/10.1103/PhysRevLett.120.232502

[12] **WMAP** Collaboration, G. Hinshaw et al., Nine-Year Wilkinson Microwave Anisotropy Probe (WMAP) Observations: Cosmological Parameter Results. Astrophys. J. Suppl. **208** (2013) 19. https://doi.org/10.1088/0067-0049/208/2/19

[13] **Planck** Collaboration, N. Aghanim et al., Planck 2018 results. VI. Cosmological parameters. https://doi.org/10.1051/0004-6361/201833910

[14] S. Tulin and H.-B. Yu, Dark Matter Self-interactions and Small Scale Structure. Phys. Rept. **730** (2018) 1–57. https://doi.org/10.1016/j.physrep.2017.11.001

[15] J. S. Bullock and M. Boylan-Kolchin, Small-Scale Challenges to the λ_dCDM Paradigm. Ann. Rev. Astron. Astrophys. **55** (2017) 343–387. https://doi.org/10.1146/annurev-astro-091916-055230

[16] D. N. Spergel and P. J. Steinhardt, Observational evidence for selfinteracting cold dark matter. Phys. Rev. Lett. **84** (2000) 3760–3763. https://doi.org/10.1103/PhysRevLett.84.3760

[17] E. D. Carlson, M. E. Machacek, and L. J. Hall, Self-interacting dark matter. Astrophys. J. **398** (1992) 43–52.

[18] A. A. de Laix, R. J. Scherrer, and R. K. Schaefer, Constraints of selfinteracting dark matter. Astrophys. J. **452** (1995) 495. https://doi.org/10.1086/176189

[19] M. R. Buckley and P. J. Fox, Dark Matter Self-Interactions and Light Force Carriers. Phys. Rev. D **81** (2010) 083522. https://doi.org/10.1103/PhysRevD.81.083522

[20] J. L. Feng, M. Kaplinghat, and H.-B. Yu, Halo Shape and Relic Density Exclusions of Sommerfeld-Enhanced Dark Matter Explanations of Cosmic Ray Excesses. Phys. Rev. Lett. **104** (2010) 151301. https://doi.org/10.1103/PhysRevLett.104.151301

[21] J. L. Feng, M. Kaplinghat, H. Tu, and H.-B. Yu, Hidden Charged Dark Matter. JCAP **07** (2009) 004. https://doi.org/10.1088/1475-7516/2009/07/004

[22] A. Loeb and N. Weiner, Cores in Dwarf Galaxies from Dark Matter with a Yukawa Potential. Phys. Rev. Lett. **106** (2011) 171302. https://doi.org/10.1103/PhysRevLett.106.171302

[23] J. Zavala, M. Vogelsberger, and M. G. Walker, Constraining Self-Interacting Dark Matter with the Milky Way's dwarf spheroidals. Mon. Not. Roy. Astron. Soc. **431** (2013) L20–L24. https://doi.org/10.1093/mnrasl/sls005

[24] M. Vogelsberger, J. Zavala, and A. Loeb, Subhaloes in Self-Interacting Galactic Dark Matter Haloes. Mon. Not. Roy. Astron. Soc. **423** (2012) 3740. https://doi.org/10.1111/j.1365-2966.2012.20912.x

[25] T. Bringmann, F. Kahlhoefer, K. Schmidt-Hoberg, and P. Walia, Strong constraints on self-interacting dark matter with light mediators. Phys. Rev. Lett. **118** (2017), no. 14 141802. https://doi.org/10.1103/PhysRevLett.118.141802

[26] M. Kaplinghat, S. Tulin, and H.-B. Yu, Dark Matter Halos as Particle Colliders: Unified Solution to Small-Scale Structure Puzzles from Dwarfs to Clusters. Phys. Rev. Lett. **116** (2016), no. 4 041302. https://doi.org/10.1103/PhysRevLett.116.041302

[27] A. Kamada, H. J. Kim, and T. Kuwahara, Maximally self-interacting dark matter: models and predictions. JHEP **20** (2020) 202. https://doi.org/10.1007/JHEP01(2020)202

[28] L. G. van den Aarssen, T. Bringmann, and C. Pfrommer, Is dark matter with long-range interactions a solution to all small-scale problems of ΛCDM cosmology? Phys. Rev. Lett. **109** (2012) 231301. https://doi.org/10.1103/PhysRevLett.109.231301

[29] S. Tulin, H.-B. Yu, and K. M. Zurek, Beyond Collisionless Dark Matter: Particle Physics Dynamics for Dark Matter Halo Structure. Phys. Rev. D **87** (2013), no. 11 115007. https://doi.org/10.1103/PhysRevD.87.115007

[30] M. Dutta, S. Mahapatra, D. Borah, and N. Sahu, Self-interacting Inelastic Dark Matter in the light of XENON1T excess. Phys. Rev. D **103**, 095018 (2021). https://doi.org/10.1103/PhysRevD.103.095018

[31] D. Borah, M. Dutta, S. Mahapatra, and N. Sahu, Boosted Self-Interacting Dark Matter and XENON1T Excess. http://arxiv.org/abs/2107.13176

[32] D. Borah, M. Dutta, S. Mahapatra, and N. Sahu, Self-interacting Dark Matter via Right Handed Neutrino Portal. Phys. Rev. D **105**, 015004 (2022). https://doi.org/10.1103/PhysRevD.105.015004

[33] D. Borah, M. Dutta, S. Mahapatra, and N. Sahu, Singlet-Doublet Self-interacting Dark Matter and neutrino Mass. http://arxiv.org/abs/2112.06847

[34] M. Dutta, N. Narendra, N. Sahu, S. Shil, Asymmetric self-interacting dark matter via Dirac leptogenesis. Phys. Rev. D **106** , 095017 (2022). https://doi.org/10.1103/PhysRevD.106.095017

[35] M. Dutta, S. Mahapatra, Mini-review on self-interacting dark matter. Eur. Phys. J. Spec. Top. (2024). https://doi.org/10.1140/epjs/s11734-024-01121-6

[36] K. Dick, M. Lindner, M. Ratz and D. Wright, Phys. Rev. Lett. 84, 4039 (2000).

[37] D. G. Cerdeno, A. Dedes and T. E. J. Underwood, The Minimal Phantom Sector of the Standard Model: Higgs Phenomenology and Dirac Leptogenesis. JHEP **0609**, 067 (2006). https://doi.org/10.1088/1126-6708/2006/09/067

[38] P. H. Gu and H. J. He, Neutrino Mass and Baryon Asymmetry from Dirac Seesaw. JCAP **0612**, 010 (2006). https://doi.org/10.1088/1475-7516/2006/12/010

[39] P. H. Gu, H. J. He and U. Sarkar, Realistic neutrinogenesis with radiative vertex correction. Phys. Lett. B **659**, 634 (2008). https://doi.org/10.1016/j.physletb.2007.11.061

[40] H. Murayama and A. Pierce, Realistic Dirac leptogenesis. Phys. Rev. Lett. **89**, 271601 (2002). https://doi.org/10.1103/PhysRevLett.89.271601

[41] C. Arina and N. Sahu, Asymmetric Inelastic Inert Doublet Dark Matter from Triplet Scalar Leptogenesis. Nucl. Phys. B **854**, 666 (2012). https://doi.org/10.1016/

j.nuclphysb.2011.09.014

[42] C. Arina, J. O. Gong and N. Sahu, Unifying darko-lepto-genesis with scalar triplet inflation. Nucl. Phys. B **865**, 430 (2012). https://doi.org/10.1016/j.nuclphysb.2012.07.029

[43] C. Arina, R. N. Mohapatra and N. Sahu, Co-genesis of Matter and Dark Matter with Vector-like Fourth Generation Leptons. Phys. Lett. B **720**, 130 (2013). https://doi.org/10.1016/j.physletb.2013.01.059

[44] J. McDonald, N. Sahu and U. Sarkar, Type-II Seesaw at Collider, Lepton Asymmetry and Singlet Scalar Dark Matter. JCAP **0804**, 037 (2008). https://doi.org/10.1088/1475-7516/2008/04/037

[45] J. Heeck, Leptogenesis with Lepton-Number-Violating Dirac Neutrinos. Phys. Rev. D **88**, 076004 (2013). https://doi.org/10.1103/PhysRevD.88.076004

[46] E. Ma and U. Sarkar, Neutrino masses and leptogenesis with heavy Higgs triplets. Phys. Rev. Lett. **80** (1998) 5716–5719. https://doi.org/10.1103/PhysRevLett.80.5716

[47] **CRESST** Collaboration, A. Abdelhameed et al., First results from the CRESST-III low-mass dark matter program. Phys. Rev. D **100** (2019), no. 10 102002. https://doi.org/10.1103/PhysRevD.100.102002

[48] **XENON** Collaboration, E. Aprile et al., Dark Matter Search Results from a One Ton-Year Exposure of XENON1T. Phys. Rev. Lett. **121** (2018), no. 11 111302. https://doi.org/10.1103/PhysRevLett.121.111302

[49] S. Tulin, H.-B. Yu, and K. M. Zurek, Resonant Dark Forces and Small Scale Structure. Phys. Rev. Lett. **110** (2013), no. 11 111301. https://doi.org/10.1103/PhysRevLett.110.111301

[50] S. A. Khrapak, A. V. Ivlev, G. E. Morfill, and S. K. Zhdanov, Scattering in the Attractive Yukawa Potential in the Limit of Strong Interaction. Phys. Rev. Lett. **90** (2003), no. 22 225002. https://doi.org/10.1103/PhysRevLett.90.225002